Robust stabilization loop design for gimbaled electro-optical imaging system

Mehmet Baskın¹ and Kemal Leblebicioğlu²

¹Aselsan Inc., Ankara, Turkey ²Dept. of EEE, Middle East Technical University, Ankara, Turkey

Abstract

For electro-optical imaging systems, line-of-sight stabilization against different disturbances created by mobile platforms is crucial property. The development of high resolution sensors and the demand in increased operating distances have recently increased the expectations from stabilization loops. For that reason, higher gains and larger bandwidths become necessary. As the stabilization loop satisfies these requirements for good disturbance attenuation, it must also satisfy sufficient loop stability. In gimbaled imaging systems, the main difficulties in satisfying sufficient loop stability are structural resonances and model uncertainties. Therefore, satisfying high stabilization performance in the presence of model uncertainties or modeling errors requires utilization of robust control methods. In this paper, robust LQG/LTR controller design is described for a two-axis gimbal. First, the classical LQG/LTR method is modified such that it becomes very powerful loop shaping method. Next, using this method, controller is synthesized. Robust stability and robust performance of stabilization loop is investigated by using singular value tests. The report is concluded with the experimental validation of the designed robust controller.

keywords: LQG/LTR, robust multivariable control, line-of-sight stabilization, multi-axis gimbal, loop shaping

1 Introduction

For precise pointing and tracking performance, line-of-sight (LOS) stabilization against various disturbances is essential for imaging systems. This problem is usually solved by using a high performance stabilization loop. High stabilization performance requires high gains and large bandwidths. As the stabilization loop posses these properties for good disturbance attenuation, it must also satisfy sufficient loop stability. In gimbaled imaging systems, the main difficulties in satisfying sufficient loop stability are structural resonances and model uncertainties. Therefore, satisfying high stabilization performance in the presence of model uncertainties or modeling errors requires utilization of robust control methods. In this aspect, this paper is devoted to the design of a stabilization loop for a two-axis gimbal.

Classical controller with PI and lead lag compensators was preferred in stabilization loops in the past [1, 2]. However, finding the classical controller that satisfies both stability and performance criteria is time consuming iterative procedure. Moreover, this method is insufficient in

optimality aspect. Recently, different techniques are used for better stabilization performance. Linear quadratic methods are explained in [3–5]. Moreover, the H_{∞} control methods are discussed in [5–7]. However, in most of the designs, analysis of performance change under model perturbations is missing. In gimbaled systems, structural resonances, sensor delays and nonlinear friction are typical source of the model perturbations. For that reason, the stabilization loop must be robust to satisfy good performance in the presence of model uncertainty. On the other hand, the robust control methods in [5, 8, 9] are not supported with theoretical and experimental data to validate the robustness of closed loops.

In previous LQG/LTR designs, desired loop shape is obtained by adjusting the weighting matrices or intensities of process and measurement noises. However in this paper, the design is modified such that it becomes a powerful loop shaping method [10]. In other words, the sensitivity at the plant output is successfully shaped for good disturbance rejection. After designing the controller, the robustness of the design is investigated by using theoretical results. Finally, the theoretical results are supported with experimental data to validate the robustness of the stabilization loop.

2 LQG/LTR control

Traditional LQG control method assumes that the plant is linear time invariant, measurement and process noises are stochastic with known statistical properties [10]. The plant is represented with a state space representation in (1),

$$\dot{x} = Ax + Bu + \Gamma w_d
y = Cx + w_n$$
(1)

where w_d and w_n are uncorrelated zero mean white noise processes having constant power spectral densities W and V as illustrated in (2).

$$E\left\{w_d(t)w_d^T(\tau)\right\} = W\delta(t-\tau), \ E\left\{w_n(t)w_n^T(\tau)\right\} = V\delta(t-\tau), \ E\left\{w_d(t)w_n^T(\tau)\right\} = 0 \quad (2)$$

The objective of the LQG theory is to minimize the cost function given in (3) where $Q = Q^T \ge 0$ and $R = R^T > 0$ are weighting matrices. The solution of this problem can be obtained in two steps:

$$J = \lim_{T \to \infty} E\left\{ \int_0^T (x^T Q x + u^T R u) dt \right\}$$
 (3)

Step 1: Obtain an optimal estimate \hat{x} of states x such that $E\left\{(x-\hat{x})^T(x-\hat{x})\right\}$ is minimized. Step 2: Use estimate as if it were true state measurement and solve LQ regulator problem.

The solutions of these two problems, Kalman filter and LQ regulator, both have very good stability properties individually. It is reported in [10, 11] that Kalman filter and LQ regulator can tolerate gain variation between $(1/2,\infty)$ and phase variation less than 60° in each channel. However when they are combined, there is no guaranteed stability conditions for LQG regulators. Moreover, LQG regulators may suffer from poor stability margins if the designers do not pay enough attention [12].

Loop transfer recovery method introduced in [13] overcomes this drawback of LQG regulators. In this method, optimal state feedback is designed such that the Kalman filter properties are recovered at the plant output. The procedure can be summarized as below where the notation

 $\Phi = (sI - A)^{-1}$ is used:

Step 1: By adjusting the covariance matrices W and V, design a Kalman filter such that the desired open loop transfer matrix $C\Phi K_f$ is obtained.

Step 2: Design a LQ regulator by choosing Q = I and $R = \rho I$, and reduce ρ until the open loop transfer matrix at the plant output approaches enough to $C\Phi K_f$ over necessary frequency interval [10].

Obtaining a good Kalman filter open loop $C\Phi K_f$ is not an easy task. Now, very effective and simple procedure that gives a good Kalman filter shape will be discussed.

2.1 Shaping singular values

To design a satisfactory Kalman filter open loop, designer should modify W and V. However, if frequency dependent weighting matrices W(s) and V(s) are used, to obtain a good $C\Phi K_f$ is simpler. In this work, this powerful and simple loop shaping technique reported in [14] is used.

Assume that as in Figure 1, instead of state disturbances the plant has a disturbance d having power spectral density D(s) and measurement noise v having power spectral density V(s). Moreover let the disturbance d and measurement noise v are created from the processes (4) and (5) respectively,

$$\dot{\xi} = A_d \xi + B_d \tilde{d}
d = C_d \xi$$
(4)

$$\dot{\eta} = A_v \eta + B_v \tilde{v}
v = C_v \eta + \Theta$$
(5)

where \tilde{d} , \tilde{v} and Θ are white noise processes. If one combines the states of the original plant and these two processes, augmented system shown in (6) is obtained.

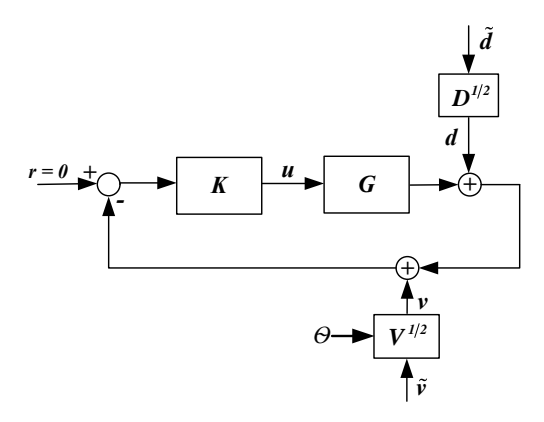


Figure 1: Plant augmentation

$$\begin{bmatrix} \dot{x} \\ \dot{\xi} \\ \dot{\eta} \end{bmatrix} = \begin{bmatrix} A & 0 & 0 \\ 0 & A_d & 0 \\ 0 & 0 & A_v \end{bmatrix} \begin{bmatrix} x \\ \xi \\ \eta \end{bmatrix} + \begin{bmatrix} B \\ 0 \\ 0 \end{bmatrix} u + \begin{bmatrix} 0 & 0 \\ B_d & 0 \\ 0 & B_v \end{bmatrix} \begin{bmatrix} \tilde{d} \\ \tilde{v} \end{bmatrix}$$

$$y = \begin{bmatrix} C & C_d & C_v \end{bmatrix} \begin{bmatrix} x \\ \xi \\ \eta \end{bmatrix} + \Theta$$

$$z = \begin{bmatrix} C & C_d & C_v \end{bmatrix} \begin{bmatrix} x \\ \xi \\ \eta \end{bmatrix}$$
(6)

The modified plant can still be used in LQG framework by assuming (7) is satisfied. In other words, LQG compensator can be designed for this augmented bigger plant in (6).

$$E\left\{\Theta(t)\Theta^{T}(\tau)\right\} > 0, \ E\left\{\Theta(t)\tilde{v}^{T}(\tau)\right\} = 0, \ E\left\{\Theta(t)\tilde{d}^{T}(\tau)\right\} = 0 \tag{7}$$

For the structure in Figure 1, the closed loop equations (8) and (9) are used.

$$z = S_o d - T_o v \tag{8}$$

$$u = -KS_0 d - KS_0 v \tag{9}$$

If the designer apply the LTR procedure for augmented plant, the cost of the LTR procedure approaches (10) by taking Q = I, $R = \rho I$ and by reducing ρ [14].

$$\lim_{\rho \to 0} J_{LTR} = \frac{1}{2\pi} \left\{ \int_{-\infty}^{\infty} \sum_{i=1} \sigma^2 [S_o D^{1/2}(jw)] + \sum_{i=1} \sigma^2 [T_o V^{1/2}(jw)] dw \right\}$$
(10)

It can be seen that LTR procedure applied at plant output trades off the output sensitivity $S_o(jw)$ against the output complementary sensitivity $T_o(jw)$ with a factor $W_e(jw) = D^{1/2}(jw)V^{-1/2}(jw)$. After assuming V = I and choosing $D^{1/2}(jw)$ appropriately, it is possible to shape the sensitivity function over required frequency ranges for good disturbance rejection [10].

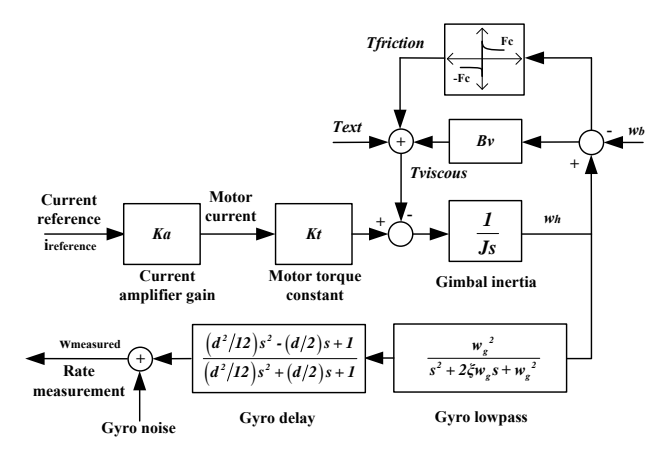


Figure 2: Gimbal model for one axis

Table 1: Parameters of the system

Parameters	Values
current aplifier gain, K_a	2 A/A
motor torque constant, K_t	$2.18 \ Nm/A$
natural frequency of rate gyro, w_g	$1646 \; rad/s$
damping of gyro, ξ	0.8
gyro delay, d	4.5~ms

3 Two-axis gimbal model

The dynamic equations of the azimuth-elevation gimbal show that when the gimbal is designed to be mass balanced, the azimuth and elevation equations decouple [15, 16]. In other words, the angular rate of any axis depends only on the net torque applied to that axis, and for one axis model given in Figure 2 can be used. By assuming that the dynamic friction only depends on inertial rate and neglecting the static friction, the model used for stabilization is approximated as in (11) [15].

$$G(s) = \frac{w_{measured}}{i_{reference}} = \frac{K_a K_t}{Js + B_v} \times \frac{w_g^2}{s^2 + 2\xi w_g s + w_g^2} \times \frac{(d^2/12)s^2 - (d/2)s + 1}{(d^2/12)s^2 + (d/2)s + 1}$$
(11)

From the datasheets of the motor, driver and gyro, the parameters listed in Table 1 are obtained. According to model (11), inertia J and viscous constant B_v need to be found. Determination of inertia J and viscous constant B_v is not easy task and it requires more complicated analysis.

3.1 Extended Kalman filter for parameter estimation

The parameter identification method through state augmentation is nonlinear, and nonlinear filtering technique needs to be utilized. In this paper, extended Kalman filter (EKF) which is the most common nonlinear filtering technique is used for unknown parameters estimation.

3.1.1 Problem simplification

While using continuous-discrete extended Kalman filter (CD-EKF), at the time update stage, the states and entries of covariance matrices are found solving differential equations. In this aspect, to solve the parameter identification problem, it is necessary to keep the model as simple as possible. To get rid of the singularity problems in numerical solution of differential equations, the delay is approximated with a first order low pass filter as in (12). This assumption is only valid when the system is excited with a low frequency signal where the magnitude and phase responses of these two transfer functions are very close.

$$\frac{(d^2/12)s^2 - (d/2)s + 1}{(d^2/12)s^2 + (d/2)s + 1} \approx \frac{1}{ds + 1}$$
(12)

Figure 3 illustrates that approximation of second order Pade with a first order transfer function gives very small magnitude errors at 4 Hz by preserving the phase information. Since the gimbal excitation is made with 4 Hz sinusoidal signal, using first order low pass instead of second order Pade gives very accurate result and saves a lot of computation effort [15]. So, the approximated

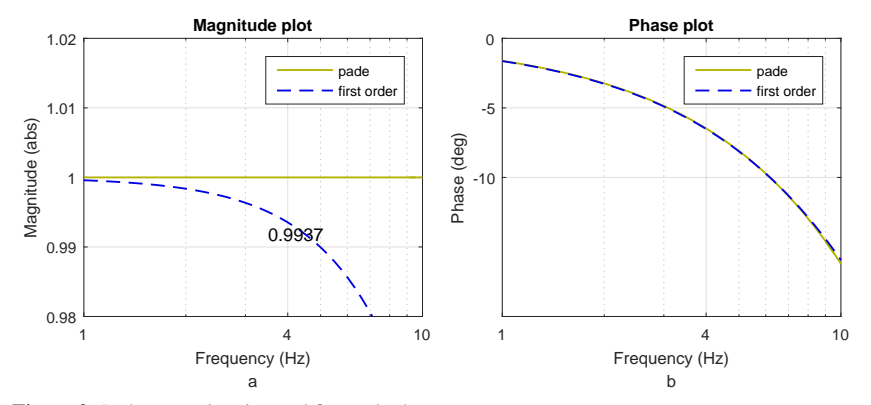


Figure 3: Pade approximation and first order low pass a Magnitude plot b Phase plot

transfer function and state space representation of the gimbal at 4 Hz are given in (13) and (14), respectively. Since J and B_v are unknown, they can be considered as fifth and sixth state. This state augmentation leads to new nonlinear model in (15).

$$G(s) \approx \frac{K_a K_t}{J_s + B_v} \times \frac{w_g^2}{s^2 + 2\xi w_q s + w_g^2} \times \frac{1}{ds + 1}$$

$$\tag{13}$$

$$\dot{x} = \begin{bmatrix}
0 & 1 & 0 & 0 \\
-w_g^2 & -2\xi w_g & w_g^2 & 0 \\
0 & 0 & -B_v/J & K_t/J \\
0 & 0 & 0 & -1/d
\end{bmatrix} x + \begin{bmatrix}
0 \\
0 \\
0 \\
1/d
\end{bmatrix} u$$

$$y = \begin{bmatrix} 1 & 0 & 0 & 0 \end{bmatrix} x$$
(14)

$$\dot{x} = \begin{bmatrix} x_2 \\ -w_g^2 x_1 - 2\xi w_g x_2 + w_g^2 x_3 \\ (-x_6 x_3 + K_t x_4)/x_5 \\ (-x_4 + u)/d \\ 0 \\ 0 \end{bmatrix}, y = x_1, x_5 = J, x_6 = B_v$$
 (15)

Observe that the gimbal model is continuous and the measurements are discrete. In this aspect, continuous-discrete EKF (CD-EKF) is considered. The detailed explanation of the CD-EKF can be found in [15, 17]. By using CD-EKF and model in (15) the unknown parameters are estimated, and online results are illustrated in Figure 4. The parameters in Table 2 is used for nominal plant construction.

3.2 Nominal model construction

The linearized two-axis gimbal can be represented with (16) where w_{az} , w_{el} , i_{az} and i_{el} are the azimuth and elevation angular rates and current inputs to corresponding axes' motors.

$$\begin{bmatrix} w_{az} \\ w_{el} \end{bmatrix} = \begin{bmatrix} G_{11} & G_{12} \\ G_{21} & G_{22} \end{bmatrix} \begin{bmatrix} i_{az} \\ i_{el} \end{bmatrix}$$
 (16)

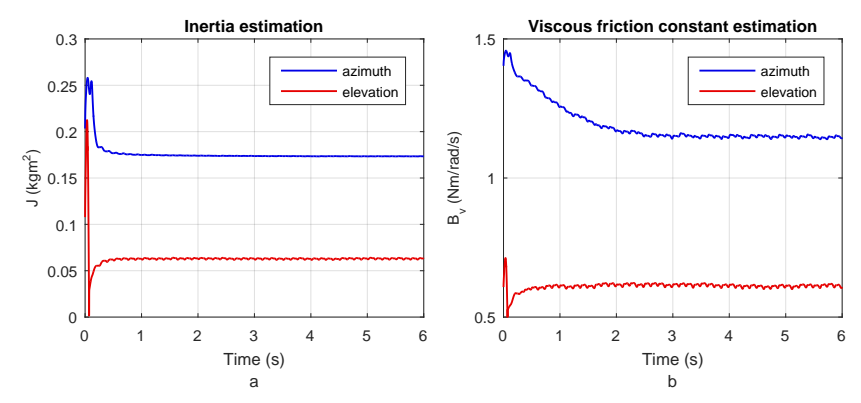


Figure 4: CD-EKF results a Inertia estimation b Viscous friction constant estimation

viscous iliction constant estimation

Table 2: Estimated parameters of the system

Parameters	Values
azimuth inertia, J	$0.1736 \ kgm^2$
azimuth viscous friction, B_v	$1.15\ Nm/(rad/s)$
elevation inertia, J	$0.063~kgm^2$
elevation viscous friction, B_v	$0.61\;Nm/(rad/s)$

 G_{11} and G_{22} are the transfer matrices of azimuth and elevation respectively having form given in (11) and parameters given in Table 1 and 2. G_{12} and G_{21} transfer matrices are approximately zero when the gimbal is mass balanced. In the actual system, gains of these transfer functions are indeed small and can be neglected [15]. In short, the MIMO nominal model for two-axis gimbal is constructed and it will be used in the next sections.

4 Design descriptions

4.1 Sensitivity weight selection

Main objective of the LOS stabilization is to minimize the pointing error due to platform motions. In electro-optical imaging systems root mean square (RMS) of the LOS error must be smaller than the single detector pixel radiation angle for clear image acquisition. For that reason, correct output sensitivity function which satisfies this constraint is found.

$$S^{-1} = \frac{(s^2/M_s + 2\xi w_b s/\sqrt{M_s} + w_b^2)}{(s^2 + 2\xi w_b s\sqrt{\epsilon} + w_b^2 \epsilon)}, M_s = 1, \epsilon = 0.01, \xi = 0.5, w_b = 2\pi 10$$
 (17)

The sensitivity function given in (17) gives approximately 75 microradian RMS LOS error under the known disturbance profile. Since this value is smaller than 100 microradian pixel radiation angle, the sensitivity in (17) is good aim for stabilization loop design. Therefore, the sensitivity weight given in (18) can be used for one axis. Similarly, for MIMO system, sensitivity weight in (19) can be used in plant augmentation stage as discussed in Section 2.

$$w_e = \frac{(s^2/M_s + 2\xi w_b s/\sqrt{M_s} + w_b^2)}{(s^2 + 2\xi w_b s/\epsilon + w_b^2\epsilon)}, M_s = 3.162, \epsilon = 0.01, \xi = 0.5, w_b = 2\pi 10$$
 (18)

$$W_e = \begin{bmatrix} w_e & 0\\ 0 & w_e \end{bmatrix} \tag{19}$$

4.2 Uncertainty weight selection

In this paper, output multiplicative uncertainty representation is used for model set representation. Firstly, the frequency response data of the gimbals are obtained by using swept sine tests at different excitation levels and at different gimbal positions. Next, using the nominal model, possible multiplicative errors are found. Finally, the stable transfer functions which upper bound all these errors are obtained. The uncertainty upper bounds for azimuth and elevation axes in (20) and (21) are used while evaluating the robustness of the stabilization loop [15]. For MIMO system, the transfer matrix in (22) is used.

$$w_{1a} = \frac{1.87s^2 + 792.65s + 90750}{s^2 + 650.35s + 572624}$$
 (20)

$$w_{1e} = \frac{1.12s^2 + 2564.28s + 289957}{s^2 + 2059.65s + 2375266}$$
 (21)

$$W_e = \begin{bmatrix} w_{1a} & 0\\ 0 & w_{1e} \end{bmatrix} \tag{22}$$

By looking at the transfer functions (20) and (21), it can be seen that at low frequencies the uncertainties are around 0.15 and 0.12 for azimuth and elevation axes respectively. At high frequencies due to the structural resonances of the gimbals, the uncertainties exceed 1 around 100 Hz and 200 Hz for azimuth and elevation axes respectively.

5 LQG/LTR design

As discussed in previous section, the transfer matrix W_e which reflects the power spectrum of output disturbance d, is of order 4. Moreover, the nominal model constructed is of order 10. For that reason, the augmentation leads to generalized plant of order 14. Hence the corresponding LQG/LTR controller will have an order of 14. Now, the LQG/LTR designs are investigated in detail.

5.1 Design 1

The LQG/LTR controller is designed by using the procedure in Section 2. As discussed previously, the aim is such that the open loop transfer matrix GK_{LQG} needs to approach to Kalman filter open loop transfer matrix $C\Phi K_f$. First, the Kalman filter is designed for augmented plant. Next, by reducing ρ , different optimal state feedbacks are designed, and the resulting open loop gains are given in Figure 5. As given in Figure 5, the recovery procedure does not achieve the objectives successfully even if one continuously reduces ρ . The main result behind this fact is the non-minimum phase behavior of the gimbal. For successful loop recovery the plant zeros are usually canceled by the compensator poles [10]. Since this is not possible for non-minimum phase plants, the procedure success reduces. To get rid of this drawback, the design 1 is reconsidered and design 2 is made.

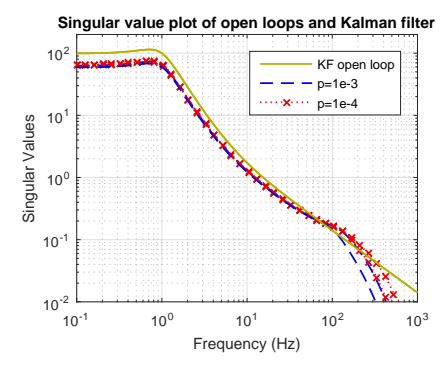


Figure 5: Singular value plot of open loops and Kalman filter for design 1

5.2 Design 2

For design 2, the transfer matrix W_e is modified such that it has a higher bandwidth and a dc gain. For this case, the Kalman filter from two designs and modified weight W_e is plotted in Figure 6a. Then different optimal state feedbacks are designed by reducing ρ , and the resulting open loop singular values are given in Figure 6b.

Observe that, for non-minimum phase plants exact recovery is not possible. However, by augmenting the plant with a new weight and demanding more performance, the design that is better than design 1 can be obtained. In other words, while trying to recover Kalman filter of design 2, it is possible to recover Kalman filter of design 1 approximately. As given in Figure 6b, the recovery procedure is made such that the objectives of the design 1 are recovered. To do that, the weighting matrix is modified such that the bandwidth is enlarged to 15 Hz from 10 Hz, and 2.5 multiples of the dc gain is used.

6 Robustness analysis with singular value tests

The aim of the stabilization loop is to satisfy disturbance rejection constraint for all models in the output multiplicative model set. For that reason, the structure in Figure 7 is used for robustness

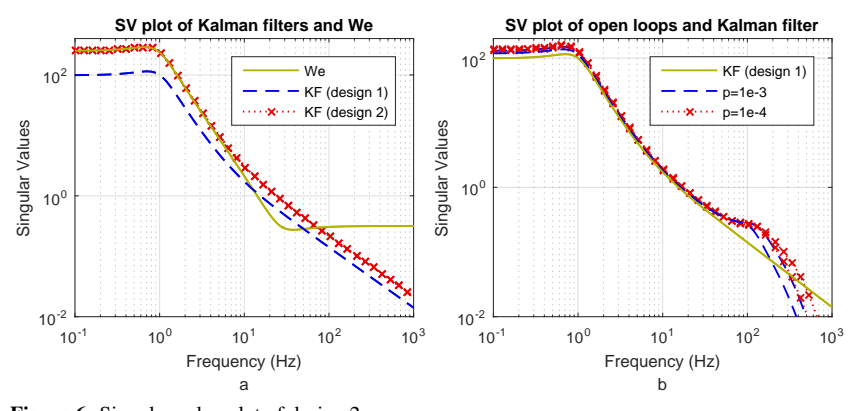


Figure 6: Singular value plot of design 2 a Singular value plot of Kalman filters and W_e for design 2 b Singular value plot of open loops and Kalman filter for design 2

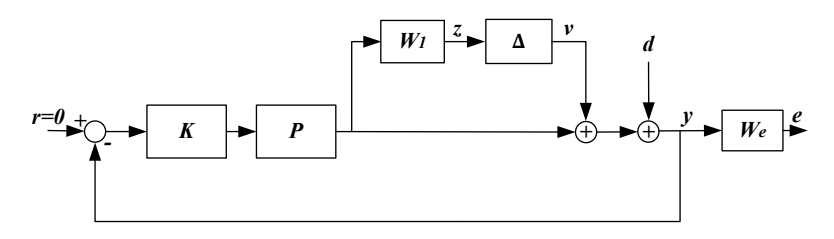


Figure 7: Structure for robustness analysis

analysis. Figure 7 shows that performance index is measured at plant output and there is only one uncertainty block in the structure. For this special structure, the robustness can be evaluated using just singular value tests, and there is no need to investigate structured singular value (μ). The nominal performance, robust stability and robust performance tests are given in (23) to (25) respectively [18, 19].

$$||W_e S_o||_{\infty} < 1 \tag{23}$$

$$||W_1 T_o||_{\infty} < 1 \tag{24}$$

$$\bar{\sigma}(W_e S_o) + \bar{\sigma}(W_1 T_o) < 1, \forall w \tag{25}$$

Observe that the structure is very special such that the robust performance test is just an addition of nominal performance and robust stability tests. Since the recovery is not satisfied for design 1, these tests are applied only to design 2. Figure 8 shows that with controllers in design 2, nominal performance and robust stability are satisfied for both ρ values. Since the peak value of robust performance test is very close to 1, robust performance can be assumed to be satisfied for $\rho=1e^{-4}$. For $\rho=1e^{-3}$ the robust performance is not satisfied; however, it leads to more stable loop. In short, reducing ρ makes the performance better at the cost of reducing stability. This situation results from the high controller gains at high frequencies for small ρ value.

7 Implementation

The LQG/LTR controller obtained with $\rho=1e^{-4}$ is selected since it approximately satisfies the robust performance. This controller is of order 14. To reduce the process cost of the implementation, reduced order controller is obtained with Balanced Truncation method. The reduced order controller is of order 12 and does not yield any performance degradation [15]. Next, this reduced order controller is discretized with bilinear transform and implemented in digital computer.

8 Experimental Results

The equation of the classical closed loop system is given in (26). If reference r, noise n and input disturbance d_i are assumed to be zero, simple equation in (27) is obtained for a two-axis gimbal.

$$y = T_o(r - n) + S_o P d_i + S_o d$$
(26)

$$\begin{bmatrix} w_{az} \\ w_{el} \end{bmatrix} = \begin{bmatrix} S_{o11} & S_{012} \\ S_{o21} & S_{o22} \end{bmatrix} \begin{bmatrix} d_{az} \\ d_{el} \end{bmatrix}$$
 (27)

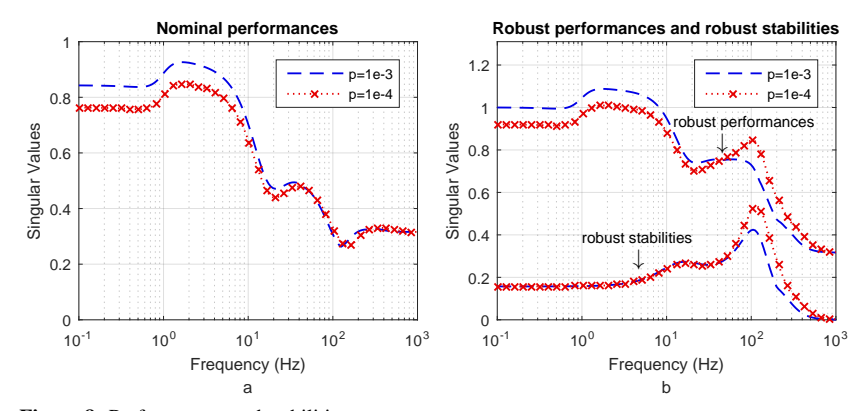


Figure 8: Performances and stabilities a Nominal performances

b Robust performances and robust stabilities

Using discretized reduced order controller, the closed loop is constructed. Next, closed loop sensitivity responses are obtained by using swept sine tests. By making d_{el} zero, S_{o11} and S_{o21} are determined by looking at w_{az} and w_{el} respectively. Similarly, under zero d_{az} , S_{o12} and S_{o22} are found. After finding responses of corresponding transfer functions, for two-input two-output system transfer matrix is constructed. Then the singular values of the sensitivity matrix are obtained and shown in Figure 9a. After that, the performance $\|W_eS_o\|_{\infty}$ is evaluated and illustrated in Figure 9b for different model perturbations.

The theoretical performances were given in Figure 8 before. The experimental results possess similar characteristics. Figure 9 shows that the sensitivity is successfully shaped and the robust performance is approximately satisfied.

9 Conclusion

The theoretical and experimental results show that with the introduced LQG/LTR method the sensitivity shaping is simple and efficient. Moreover, the designed closed loop gives good results for both nominal model and any model in the model set. All results show that when the performance is measured only by sensitivity, LQG/LTR method can satisfy the robust performance. However,

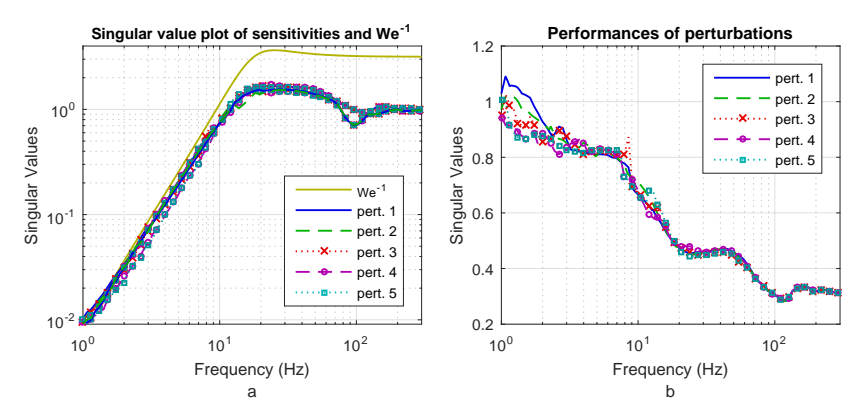


Figure 9: Experimental results a Singular value plot of sensitivities and W_e^{-1} b Performances of perturbations

when more sophisticated performance index is available, LQG/LTR method can be insufficient [15].

10 Acknowledgments

The support and facilities provided by ASELSAN Inc. are gracefully appreciated.

References

- [1] P. Kennedy and R. Kennedy, Line of sight stabilization primer. Peter Kennedy, 2013.
- [2] M. K. Masten, "Inertially stabilized platforms for optical imaging systems," *Control Systems*, *IEEE*, vol. 28, no. 1, pp. 47–64, 2008.
- [3] W. J. Bigley and V. J. Rizzo, "Wideband linear quadratic control of a gyro-stabilized electro-optical sight system," *Control Systems Magazine*, *IEEE*, vol. 7, no. 4, pp. 20–24, 1987.
- [4] R. Marathe, "Design of the line of sight stabilization using lqg/ltr methodology for mobile land vehicles," Master's thesis, Indian Institute of Technology, 1997.
- [5] H. P. Lee, "Scan loop control design for a spin-stabilised seeker," in *Control Theory and Applications, IEE Proceedings*-, vol. 145, no. 2. IET, 1998, pp. 119–126.
- [6] J. K. Moorty, R. Marathe *et al.*, "H∞ control law for line-of-sight stabilization for mobile land vehicles," *Optical Engineering*, vol. 41, no. 11, pp. 2935–2944, 2002.
- [7] Z. Liu, Q. Bao, Y. Xia, and X. Liu, "H-infinity mix sensitivity controller design based on gime for electro-optical stabilization and tracking system," in *ISPDI 2013-Fifth International Symposium on Photoelectronic Detection and Imaging*. International Society for Optics and Photonics, 2013, pp. 89 061Y–89 061Y.
- [8] B. Wenliang, H. Xianlin, and B. Xiaojun, "Control system design of multi-gimbal electro-optical platform by the technique of μ-synthesis," in *Control Conference (CCC)*, 2010 29th Chinese. IEEE, 2010, pp. 3447–3452.
- [9] S. Kim, S. Kim, and Y. Kwak, "Robust control for a two-axis gimbaled sensor system with multivariable feedback systems," *Control Theory & Applications, IET*, vol. 4, no. 4, pp. 539–551, 2010.
- [10] J. M. Maciejowski, Multivariable feedback design. Addison-Wesley, 1989.
- [11] B. D. Anderson and J. B. Moore, *Optimal control: linear quadratic methods*. Courier Corporation, 2007.
- [12] J. Doyle, "Guaranteed margins for lqg regulators," *IEEE Transactions on Automatic Control*, no. 4, pp. 756–757, 1978.
- [13] J. Doyle and G. Stein, "Multivariable feedback design: Concepts for a classical/modern synthesis," *IEEE Transactions on Automatic Control*, no. 1, pp. 4–16, 1981.

- [14] G. Stein and M. Athans, "The lqg/ltr procedure for multivariable feedback control design," *Automatic Control, IEEE Transactions on*, vol. 32, no. 2, pp. 105–114, 1987.
- [15] M. Baskın, "Lqg/ltr, h-infinity and mu robust controllers design for line of sight stabilization," Master's thesis, Middle East Technical University, 2015.
- [16] B. Ekstrand, "Equations of motion for a two-axes gimbal system," *Aerospace and Electronic Systems, IEEE Transactions on*, vol. 37, no. 3, pp. 1083–1091, 2001.
- [17] F. L. Lewis, L. Xie, and D. Popa, *Optimal and robust estimation: with an introduction to stochastic control theory.* CRC press, 2007, vol. 29.
- [18] K. Zhou and J. C. Doyle, *Essentials of robust control*. Prentice hall Upper Saddle River, NJ, 1998.
- [19] S. Skogestad and I. Postlethwaite, *Multivariable feedback control: analysis and design*. Wiley New York, 2007.